International Journal of Heat and Mass Transfer 66 (2013) 844–854

Contents lists available at ScienceDirect

International Journal of Heat and Mass Transfer

journal homepage: www.elsevier.com/locate/ijhmt

Local mass non-equilibrium dynamics in multi-layered porous media: application to the drug-eluting stent

Giuseppe Pontrelli [a,*], Andrea Di Mascio [a], Filippo de Monte [b]

[a] Istituto per le Applicazioni del Calcolo, CNR Via dei Taurini 19, 00185 Roma, Italy
[b] Department of Industrial and Information Engineering and Economics, University of L'Aquila, Via G. Gronchi 18, 67100 L'Aquila, Italy

ARTICLE INFO

Article history:
Received 2 November 2012
Received in revised form 15 July 2013
Accepted 15 July 2013
Available online 23 August 2013

Keywords:
Multi-phase mass transfer
Multi-layered porous media
Diffusion equation
Drug delivery
Pharmacokinetics

ABSTRACT

A solution for a model of mass diffusion from a drug-eluting stent to the arterial wall is addressed. The coating layer is described as a porous reservoir where the drug is initially loaded in polymer-encapsulated solid-phase, and then released both to the coating and to the arterial tissue in a liquid-phase. The endothelium, intima, internal elastic lamina and media are all treated as homogeneous porous media and the drug transfer through them is modelled by a non-homogeneous set of coupled partial differential equations that describe a local mass non-equilibrium diffusion problem. Drug concentration levels and mass profiles in each layer at various times are computed as a spectral decomposition: numerical results show a delayed release depending on the physico-chemical drug properties combined with the microstructure of the polymeric-coated stents.

1. Introduction

The most popular approach for the prevention of arterial restenosis consists in the insertion of a drug-eluting stent (DES), a device able to release antiproliferative drugs into arterial wall. The DES consists of a metallic wired platform coated with a polymer film that encapsulates a therapeutic drug aimed at reducing vessel remodelling. The polymeric surface can include a rate-limiting barrier that provides a more controlled release. For high performance, both the stent geometry and the coating design should be optimized. The success of an antirestenotic drug therapy from a DES is dependent on the extent of drug elution from the stent, the rate of release, accumulation of drug and receptor binding in the arterial wall [1]. The local drug concentrations achieved are directly correlated with the biological effects and local toxicity, and finding the optimum dose to be delivered to tissues still remains a challenge [2].

Many studies have been carried out about DES, on their efficacy, their optimal design, either with experimental methods [3] and with numerical simulations [4–6]. Nonetheless, many questions remain unanswered for bioengineers and clinicians who continue to explore and evaluate this technology. Several researches have been proposed to address fundamental questions of pharmacokinetics, to estimate the drug elution in the biological tissues over a period of time [7]. Validated mathematical models for computing the drug concentration in the wall can be a useful tool in the design and development of better properties of DES [8]. The model should incorporate the pharmacokinetics responsible for the drug release and can be used to study the effect of different coating parameters and configuration on the drug elution [8,9]. Hossainy and Prabhu developed a mathematical model to predict the transport reaction of drug release in biodurable materials or with degradation of biodegradable polymers [10]. Such a model has been recently extended in [11]. The multiphase release of drug from the coated stent and its distribution in the arterial wall must be carefully tailored to achieve the optimal therapeutic effect and to deliver the correct dose in the required time [12]. The pharmacological effects of the drug, tissue accumulation, duration and distribution could potentially have an effect on its efficacy and a delicate balance between adequate amount of drug delivered over an extended period of time and minimal local toxicity should be found [13]. Although a large number of mathematical models are available nowadays for drug dynamics in the wall, there is a limited effort to explain the drug elution mechanism from the coating platform. This is a very important issue indeed, since the polymer acts as a drug reservoir, and a strategical design of its characteristics would improve the release performances. It is worth to emphasize that the drug elution depends on the properties of the "coating-wall" system, taken as a whole.

In most studies, the coating is considered as a continuum where the drug is incorporated at liquid phase. As a matter of fact, at a microscopic scale, the polymer is a porous medium where solid

* Corresponding author.
E-mail addresses: giuseppe.pontrelli@gmail.com (G. Pontrelli), filippo.demonte@univaq.it (F. de Monte).

0017-9310/$ - see front matter © 2013 Elsevier Ltd. All rights reserved.
http://dx.doi.org/10.1016/j.ijheatmasstransfer.2013.07.041

Nomenclature

c	volume-averaged drug concentration in fluid phase.
$c^{s,f}$	intrinsic volume- averaged drug concentration in the phase s,f.
d^*	penetration distance.
$D^{s,f}$	effective drug diffusivity coefficient in phase s,f.
k	partition coefficient.
K_0	solid–liquid mass transfer coefficient.
l	layer thickness
M	dimensionless mass per unit of area.
P	membrane permeability coefficient.
r_h	hydraulic radius.
t	time.
t_0	characteristic solid–liquid transfer time.
x	space coordinate.
X	eigenfunction.

Greek symbols

γ	nondimensional drug diffusivity coefficient.
ϵ	porosity.
λ	eigenvalue.
ϕ	nondimensional permeability.
θ	fraction of drug mass.

Subscripts–superscripts

0	0-th layer (coating).
i	i-th wall layer.
f,s	fluid, solid phase.
n	layer number.

and fluid phases coexist [14]. In particular, the solid matrix acts as a drug reservoir, where it is initially loaded in solid phase [15]. Subsequently, after stent insertion, expansion and contact with vascular tissues, a part of the drug is first transferred in fluid-phase, at a rate depending on the porosity, permeability, and drug characteristics, and then diffused to the surrounding tissues [7].

In addition, the multi-layered structure of the wall has to be included for an accurate description of the release mechanism through the biological tissue [14]. This aspect has been recently addressed in a series of models in a hierarchy of increasing complexity [16–18] to which the reader is referred for further details. In the present work, we develop an extension of [18], where a relatively simple model for a better understanding of the drug release mechanism in the coating and its subsequent dynamics into the multi-layered wall is derived. Any other mechanical effect (i.e. compression, expansion) due to the metallic or polymeric degradation/erosion is neglected. The porous structure of the polymeric matrix leads to a two-phase representation for the drug concentration where a characteristic transfer time is defined as a function of the drug composition and coating manufacture. In a simplified model, this brings to a non-homogeneous differential problem. A semi-analytical expression is given for drug concentration and mass in each layer at various times. An alternative perturbation solution is also provided. The simulations can be used to assess experimental procedures to evaluate drug delivery efficacy, in the design of polymer-coated stents, and to provide valuable insights into local vascular drug-delivery systems.

2. The mathematical model

A drug-eluting stent (DES) consists of a tubular wire mesh (*strut*), inserted in a stenosed artery and coated with a thin layer (*coating*) of biocompatible polymeric gel containing a therapeutic drug to be delivered (Fig. 1). Drug release from a polymeric-coated stent depends on many factors, such as physical and geometrical parameters of the coating and biochemical properties of the drug. Once the drug is released into the wall, its dynamics, reaction, and absorption are depending on the characteristics of the wall layers, such as drug diffusivity [4].

Let us consider a stent coated by a thin layer (of thickness l_0) of gel containing a drug and embedded into the arterial wall. As most of the mass dynamics occurs along the direction normal to the polymeric surface (radial direction), and by assuming axial symmetry, we restrict our study to a simplified 1D model. In particular, we consider a radial line crossing the metallic strut, the coating and the arterial wall and pointing outwards and, the wall thickness being very small with respect to the arterial radius, a Cartesian coordinate system x is used along it. It is generally accepted that the arterial wall consists of a sequence of contiguous layers of different physical properties and thickness, say the endothelium, the intima, the internal elastic lamina (IEL), the media and the adventitia (see [19] for an anatomic and physiological description of them).

Without loss of generality, let us assume $x_0 = 0$ is the coating-wall interface. In a general 1D framework, let us consider a set of intervals $[x_{i-1}, x_i]$ $i = 0,1,2,\ldots,n$ having thickness $l_i = x_i - x_{i-1}$ modelling the coating (layer 0) and the wall (layers 1,2,...,n) (Fig. 2).

2.1. From microscopic to mesoscopic scale

In many studies the polymeric layer covering the stent is modeled as a biocompatible substrate where the drug is initially contained and subsequently diffused and transported in adjacent

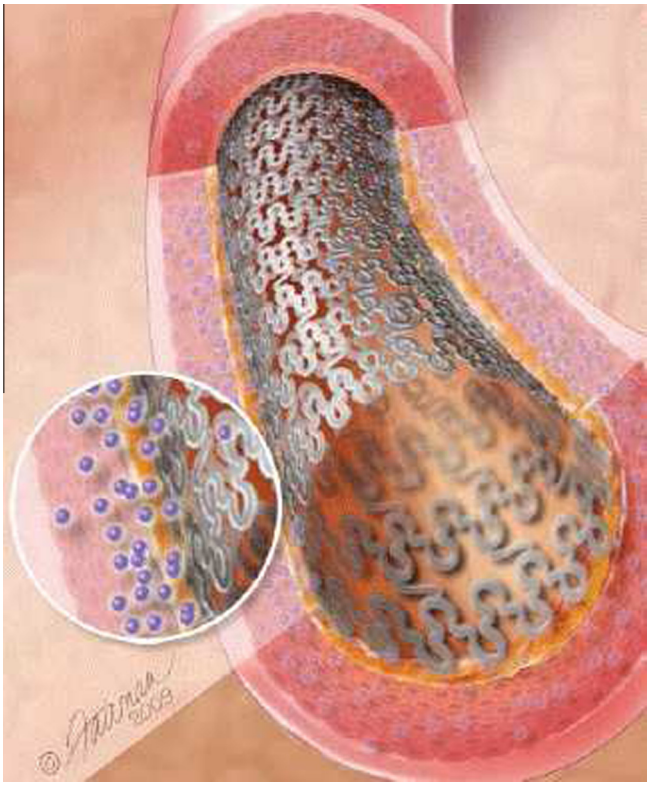

Fig. 1. A drug-eluting stent implanted in an artery.

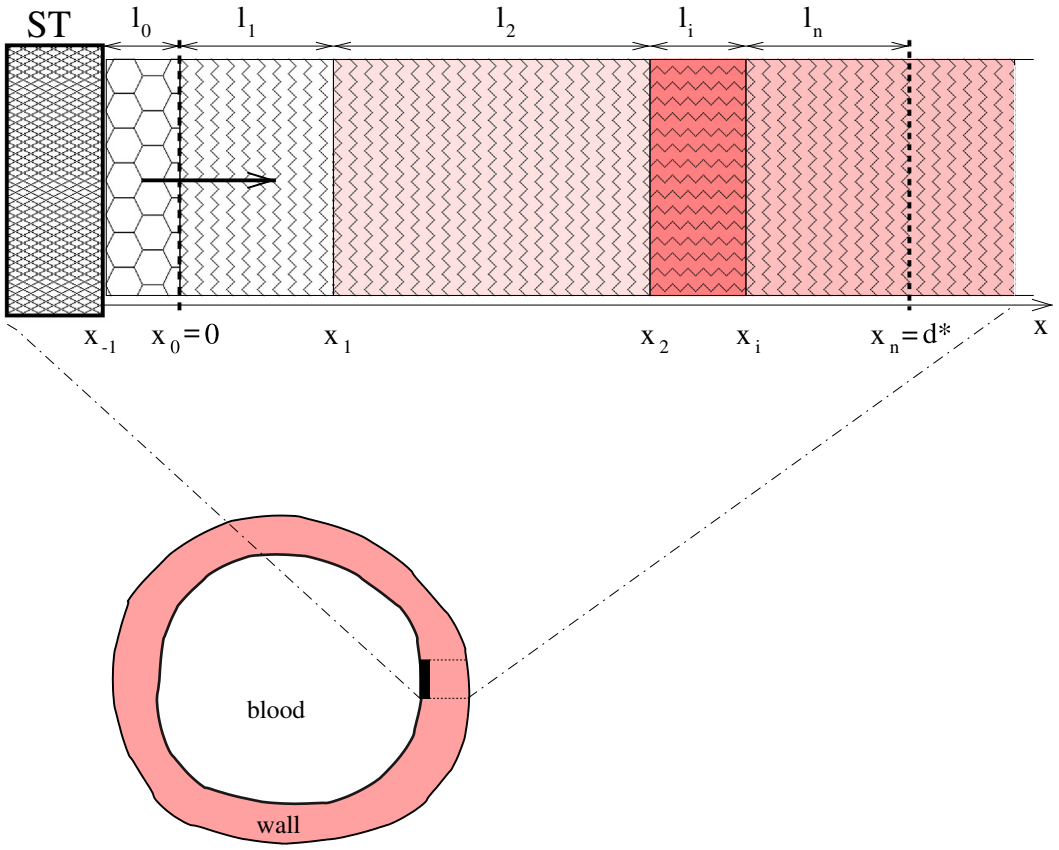

Fig. 2. A sketch of the layered wall. The 1D wall model is defined along the line normal to the strut stent surface.

wall layers. In this paper we are interested in non-local mass transfer processes in the coating, where the drug passes from solid (polymer-encapsulated) to liquid phase [15]. A microscopic approach would require the knowledge of the specific and local geometry of the individual pore structure networks, that is unfeasible. Therefore, both the polymeric matrix and the wall layers are treated as macroscopically homogeneous porous media by appropriately defining averaged variables over a sufficiently large *representative elementary volume* V_{ref} (r.e.v., for short) [7,15,20–22].

The time and length scales of the r.e.v. (mesoscale) are much larger than the pore scale (microscale), but considerably smaller than the typical length scale of the problem (macroscale). Two different ways of averaging over a volume exist. One is based on the volume of each phase contained in r.e.v., that is V^f_{ref}, for the fluid-phase[1] (which is a fraction $k\epsilon$ of the r.e.v.) and V^s_{ref} for the solid-phase (which is the fraction $1-k\epsilon$ of the r.e.v.). Another way is to average over the whole r.e.f. $V_{ref} = V^f_{ref} + V^s_{ref}$ (for more details, see subs 3.2.1.1. of [22]). In the first case, we refer to *intrinsic* volume-averaged drug concentration in fluid and solid phases c^f and c^s (μg/ml), in the second, to volume-averaged drug concentrations, $\bar{c}^f$ and $\bar{c}^s$ (μg/ml). They are related by the relationships:

$$\bar{c}^f = k\epsilon c^f \qquad \bar{c}^s = (1-k\epsilon)c^s \tag{2.1}$$

where $k\epsilon$ represents the *available volume fraction* which provides the ratio of the available volume to V^f_{ref} [7]. In detail, $\epsilon(\leqslant 1)$ is the *porosity*, that is the ratio V^f_{ref}/V_{ref}; and $k(\leqslant 1)$ is the so-called *partition coefficient* defined as the ratio of the available volume (portion of void volume that is accessible to a drug or solute) to V^f_{ref}. It can happen, in fact, that a pore is inaccessible to a solute if the size of the pore itself or of its surrounding is smaller than those of the solute molecules.

As the drug passes from solid (polymer-encapsulated) to liquid phase [15] in the coating (local mass non-equilibrium, LMNE for short) and, subsequently is transported in the arterial wall, we will not make use of the volume-averaged drug concentration $\bar{c}^s$. Thus, for the sake of brevity, $\bar{c}^f$ will be simply denoted by c and, hence, the first of Eq. (2.1) becomes:

$$c(x,t) = k\epsilon\, c^f(x,t) \tag{2.2}$$

2.2. The coating two-phase diffusion model

The coating of a DES is made of a porous polymeric matrix that encapsulates a therapeutic drug in solid phase; as such, it is unable to diffuse and to be delivered into the tissue [5]. Nevertheless, when expanded and deployed into the arterial wall, the stent coating embeds the surrounding biological fluids. As a consequence, such fluids fill the interstitial spaces of the polymer and form a network of liquid channels, acting as a release medium for the drug. Thus, a fraction of the drug mass is first transferred, in a finite time, to the liquid channels formed in the polimeric matrix, and then released and diffused into the arterial wall. We attempt to carry out a mesoscale description of the intrinsic volume-averaged drug concentrations in the liquid (c^f_0) and solid (c^s_0) phases considered separately to achieve a LMNE description. Strictly speaking, the structure of a porous medium, the flow and the mass transport processes though it, are described spatially by two or three dimensional models. However, many concepts (granularity, tortuosity, porosity) can also be represented and employed by one-dimensional models [10]. The equations governing the drug diffusion in the solid and liquid phases of the coating (layer 0) are:

[1] Superscripts *s* and *f* denote solid and fluid phases, respectively.

$$(1-k_0\epsilon_0)\frac{\partial c_0^s}{\partial t}=(1-k_0\epsilon_0)D_0^s\frac{\partial^2 c_0^s}{\partial x^2}-\frac{K_0}{r_h}k_0\epsilon_0\left(c_0^s-c_0^f\right)\ \text{ in } (-l_0,0) \quad (2.3)$$

$$k_0\epsilon_0\frac{\partial c_0^f}{\partial t}=k_0\epsilon_0 D_0^f\frac{\partial^2 c_0^f}{\partial x^2}+\frac{K_0}{r_h}k_0\epsilon_0\left(c_0^s-c_0^f\right)\ \text{ in } (-l_0,0) \quad (2.4)$$

In the above equations D_0^s (resp. D_0^f) (cm^2/s) is the effective drug diffusivity in the solid (resp. liquid) mixture of the coating, averaged over the solid (resp. liquid) phase. Both of them are *intrinsic volume averaged diffusivities*, meaning with that the diffusivity in the presence of a porous medium, which accounts for the tortuosiy of pathways and for local boundaries. Moreover, ϵ_0 is the porosity, k_0 is the partition coefficient, r_h the hydraulic radius (defined as the free-flow area over the wetted perimeter), that can be considered the mean radius of a typical pore, and K_0 the solid–fluid mass transfer coefficient (cm/s) discussed below.

By using Eq. (2.2), Eqns (2.3)–(2.4) can be rewritten as:

$$\frac{\partial c_0^s}{\partial t}=-\frac{\rho_0}{t_0}\left(c_0^s-\frac{c_0}{k_0\epsilon_0}\right)\quad \text{in } (-l_0,0) \quad (2.5)$$

$$\frac{\partial c_0}{\partial t}=D_0^f\frac{\partial^2 c_0}{\partial x^2}+\frac{k_0\epsilon_0}{t_0}\left(c_0^s-\frac{c_0}{k_0\epsilon_0}\right)\quad \text{in } (-l_0,0) \quad (2.6)$$

where the diffusion coefficient D_0^s , extremely small in general, has been neglected and:

$$\rho_0=\frac{k_0\epsilon_0}{1-k_0\epsilon_0}\qquad t_0=\frac{r_h}{K_0} \quad (2.7)$$

are, respectively, the void ratio and a characteristic solid–fluid transfer time associated with the exchange between the two phases. The latter, t_0, comes naturally from Eqs. (2.5) and (2.6) and, by definition, is a function of physico-chemical properties of the substance and of the microstructure of the porous material. The determination of an appropriate value of K_0 is a critical aspect of using LMNE approach. However, non-local theories and direct pore-scale simulations are able to estimate its value [23]. In the current case, as convection is absent in the coating, we simply have a polymeric matrix from which the solute is removed by using a stagnant liquid solvent (plasma). Because of that, $K_0=\frac{D_0^f}{r_h}$ (see Subs. 1.4.1.3 of Ref. [24]) and hence, t_0 becomes proportional to r_h^2. An order of magnitude for t_0 is one day, while some experimental data indicate a characteristic time of ten days [12].

Together with these equations the initial conditions are given:

$$c_0^s(x,0)=C_0^s\qquad c_0(x,0)=0 \quad (2.8)$$

expressing that, at initial time, the whole drug exists in the solid phase at maximum constant concentration and, subsequently, released into the liquid phase and to the wall. Since the metallic strut is impermeable to the drug, no mass flux passes through the boundary surface $x=x_{-1}=-l_0$; here we impose a no-flux condition:

$$D_0^f\frac{\partial c_0}{\partial x}=0\quad \text{at } x=-l_0 \quad (2.9)$$

Flux conditions at coating-wall interface

In the coating only the fluid phase takes part to the mass exchange with the wall (liquid phase). Let us impose the balance of flux at the coating (0) – wall (1) interface ($x=0$) for the fluid-phase:

$$D_0^f\frac{\partial c_0}{\partial x}=D_1^f\frac{\partial c_1}{\partial x}\quad \text{at } x=0 \quad (2.10)$$

In addition, a permeable membrane (called *topcoat* or *rate-limiting barrier*) is located at $x=0$ to control and sustain the drug release rate. Being much thinner than the other layers, it has not been modelled spatially, but its effect is described by means of a resistance of permeability P (cm/s) [3,10]. A continuous mass flux passes through it orthogonally to the coating film with a possible concentration jump. In the present case, the mass transfer through the topcoat can be described using the second Kedem–Katchalsky equation [25]:

$$-D_0^f\frac{\partial c_0}{\partial x}=P\left(\frac{c_0}{k_0\epsilon_0}-\frac{c_1}{k_1\epsilon_1}\right)\quad \text{at } x=0 \quad (2.11)$$

2.3. The multi-layered wall model and interface conditions

In the n layers of the wall, the drug dynamics is described in terms of the volume- averaged drug concentration in fluid phase by the following advection–diffusion–reaction equations and related initial conditions:

$$\frac{\partial c_i}{\partial t}=D_i^f\frac{\partial^2 c_i}{\partial x^2}-\delta_i\frac{\partial c_i}{\partial x}-\beta_i c_i\quad \text{in } (x_{i-1},x_i)\quad i=1,2,\ldots,n$$
$$c_i(x,0)=0 \quad (2.12)$$

where D_i^f(cm^2/s) is the effective diffusivity of drug, and δ_i(cm/s) accounts for a constant characteristic convection parameter. Since the contribution of the filtration velocity is small with respect to the other terms [17], it will be neglected.

The last term on the r.h.s. of Eq. (2.12.1) represents the drug reaction on the surface of smooth muscle cells (SMCs) inside the media layer. This is modelled by a linear term, $\beta_i>0(s^{-1})$ being an effective first order consumption rate coefficient. The spatial dependence of the reaction terms are implicitly incorporated in the multi-layered wall structure. However, it has been shown that their contribution is negligible [17]. Hence, we assume $\delta_i=\beta_i=0$ for all i.

To close the previous mass transfer system of Eq. (2.12), flux and fluid-phase concentration continuity conditions have to be assigned at each layer interface $x=x_i$:

$$\frac{c_i}{k_i\epsilon_i}=\frac{c_{i+1}}{k_{i+1}\epsilon_{i+1}}\qquad D_i^f\frac{\partial c_i}{\partial x}=D_{i+1}^f\frac{\partial c_{i+1}}{\partial x}\qquad \text{at } x=x_i$$
$$i=1,2,\ldots n-1 \quad (2.13)$$

Finally, a boundary condition has to be imposed at the limit of adventitia x_n. The concept of penetration distance d^* is useful to define the "physical limit" of the arterial wall. This is defined as the distance where the concentration and the mass flux vanish, at a given time, within a prescribed tolerance. The penetraton distance over a multi-layered medium depends on the thicknesses l_i's and the diffusion coefficients D_i's. A precise definition of it and its estimates are given in [18]. Thereby the concentration and mass flux at that point equate their initial value there, say zero, at d^* and the boundary conditions can be posed as:

$$c_n=0\quad \text{or}\quad \frac{\partial c_n}{\partial x}=0\quad \text{at } x=x_n=d^* \quad (2.14)$$

2.4. Nondimensional equations

All the variables and the parameters are now normalized to get easily computable dimensionless quantities as follows:

$$\bar{x}=\frac{x}{d^*}\qquad \bar{l}_i=\frac{l_i}{d^*}\qquad \bar{t}=\frac{D_{max}^f}{(d^*)^2}t\qquad \bar{t}_0=\frac{D_{max}^f}{(d^*)^2}t_0$$
$$\gamma_i=\frac{D_i^f}{D_{max}^f}\qquad \phi=\frac{Pd^*}{D_{max}^f}\qquad \bar{c}_i=\frac{c_i}{C_0^s} \quad (2.15)$$

where subscripts max denote maximum values across the $n+1$ layers. By omitting the bar for simplicity, the mass transfer problem

(2.5)–(2.14) can now be written in dimensionless form. The solid-phase dynamics is governed by the equation:

$$\frac{\partial c_0^s}{\partial t} = -\frac{\rho_0}{t_0}\left(c_0^s - \frac{c_0}{k_0\epsilon_0}\right) \qquad \text{in } (x_{-1},0) \tag{2.16}$$

supplemented with the initial condition:

$$c_0^s(x,0) = 1 \tag{2.17}$$

The fluid-phase concentration equations in the multi-layered medium are:

$$\frac{\partial c_0}{\partial t} = \gamma_0 \frac{\partial^2 c_0}{\partial x^2} + \frac{k_0\epsilon_0}{t_0}\left(c_0^s - \frac{c_0}{k_0\epsilon_0}\right) \quad \text{in } (x_{-1},0) \tag{2.18}$$

$$\frac{\partial c_i}{\partial t} = \gamma_i \frac{\partial^2 c_i}{\partial x^2} \quad \text{in } (x_{i-1},x_i) \quad i = 1,\ldots,n \tag{2.19}$$

with the following initial conditions:

$$c_i(x,0) = 0 \quad i = 0,1,\ldots,n \tag{2.20}$$

and the following interface and B.C.'s:

$$\begin{aligned}
&\frac{\partial c_0}{\partial x} = 0 \quad \text{at } x = x_{-1}\\
&\gamma_0 \frac{\partial c_0}{\partial x} = \gamma_1 \frac{\partial c_1}{\partial x} \quad -\gamma_0 \frac{\partial c_0}{\partial x} = \phi\left(\frac{c_0}{k_0\epsilon_0} - \frac{c_1}{k_1\epsilon_1}\right) \quad \text{at } x = 0\\
&\frac{c_i}{k_i\epsilon_i} = \frac{c_{i+1}}{k_{i+1}\epsilon_{i+1}}\\
&\gamma_i \frac{\partial c_i}{\partial x} = \gamma_{i+1}\frac{\partial c_{i+1}}{\partial x} \quad \text{at } x = x_i \quad i = 1,2,\ldots,n-1\\
&c_n = 0 \quad \text{at } x = 1
\end{aligned} \tag{2.21}$$

3. Method of solution

The Eq. (2.16) can be rewritten as

$$\frac{\partial c_0^s}{\partial t} = -h_1 c_0^s + h_2 c_0 \tag{3.1}$$

where

$$h_1 = \frac{k_0\epsilon_0}{t_0(1-k_0\epsilon_0)} \qquad h_2 = \frac{1}{t_0(1-k_0\epsilon_0)} \tag{3.2}$$

The solution of Eq. (3.1) is:

$$c_0^s(x,t) = \exp(-h_1 t) + \exp(-h_1 t)\int_0^t \exp(h_1\tau) h_2 c_0(x,\tau)\,d\tau \tag{3.3}$$

We now follow a similar approach as in Ref. [18], where the correspondent problem for $t_0 \to 0$, is solved. The solution c_i of problem (2.18)–(2.21) admits a spectral decomposition:

$$c_i(x,t) = \sum_{k=1}^{\infty} G_k(t) X_i^k(x) \quad i = 0,1,\ldots,n \tag{3.4}$$

with

$$c_i(x,0) = \sum_{k=1}^{\infty} G_k(0) X_i^k(x) = 0 \quad i = 0,1,\ldots,n \tag{3.5}$$

where the coefficient G_k have to be found, and $X_i^k = a_i \cos\left(\lambda_i^k x\right) + b_i \sin\left(\lambda_i^k x\right)$ are the eigenfunctions of the Sturm–Liouville problem as in [18] (c_i satisfy the same boundary and interface conditions, for $i = 0,1,2\ldots,n$). By replacing c_0, expressed as in (3.4), in Eq. (3.3):

$$c_0^s(x,t) = \exp(-h_1 t) + h_2 \sum_{k=1}^{\infty} H_k(t) X_0^k(x) \tag{3.6}$$

$$H_k(t) = \int_0^t G_k(\tau)\exp(h_1(\tau - t))\,d\tau \tag{3.7}$$

By replacing this expression into Eq. (2.18), by multiplying Eq. (2.18) by X_0^k, Eq. (2.19) by X_i^k, integrating across the corresponding layer, dividing by $k_i\epsilon_i$ and summing all the layer contributions, we end up with:

$$\begin{aligned}
\frac{dG_k}{dt} &= -\gamma_0\left(\lambda_0^k\right)^2 G_k + \frac{1}{N_k t_0}\left[\exp(-h_1 t)\int_{-l_0}^{0} X_0^k(x)\,dx + h_2\exp(-h_1 t)\right.\\
&\times \int_0^t \sum_{p=1}^{\infty} G_p(\tau)\left(\int_{-l_0}^{0} X_0^p(x) X_0^k(x)\,dx\right)\exp(h_1\tau)\,d\tau - \frac{1}{k_0\epsilon_0}\sum_{p=1}^{\infty} G_p(t)\\
&\left.\times \int_{-l_0}^{0} X_0^p(x) X_0^k(x)\,dx\right] = -\gamma_0\left(\lambda_0^k\right)^2 G_k + \frac{1}{N_k t_0}\left[\beta_0^k\exp(-h_1 t)\right.\\
&\left.+\sum_{p=1}^{\infty}\alpha_0^{kp}\left(h_2 H_p(t) - \frac{G_p(t)}{k_0\epsilon_0}\right)\right]\\
G_k(0) &= 0
\end{aligned} \tag{3.8}$$

where the norm

$$N_k = \sum_{i=0}^{n}\frac{1}{k_i\epsilon_i}\int_{x_{i-1}}^{x_i}\left(X_i^k\right)^2 dx$$

can be made explicit as in [18] and the spatial integrals:

$$\beta_0^k = \int_{-l_0}^{0} X_0^k(x)\,dx = -\frac{b_0^k}{\lambda_0^k}$$

$$\begin{aligned}
\alpha_0^{kh} &= \int_{-l_0}^{0} X_0^k(x) X_0^h(x)\,dx\\
&= a_0^k a_0^h \int_{-l_0}^{0} \cos\left(\lambda_0^k x\right)\cos\left(\lambda_0^h x\right)dx + a_0^k b_0^h \int_{-l_0}^{0} \cos\left(\lambda_0^k x\right)\sin\left(\lambda_0^h x\right)dx\\
&+ b_0^k a_0^h \int_{-l_0}^{0} \sin\left(\lambda_0^k x\right)\cos\left(\lambda_0^h x\right)dx + b_0^k b_0^h \int_{-l_0}^{0} \sin\left(\lambda_0^k x\right)\sin\left(\lambda_0^h x\right)dx\\
&= a_0^k a_0^h\left[\frac{\sin\left(l_0\left(\lambda_0^k - \lambda_0^h\right)\right)}{2\left(\lambda_0^k - \lambda_0^h\right)} + \frac{\sin\left(l_0\left(\lambda_0^k + \lambda_0^h\right)\right)}{2\left(\lambda_0^k + \lambda_0^h\right)}\right]\\
&+ b_0^k b_0^h\left[\frac{\sin\left(l_0\left(\lambda_0^k - \lambda_0^h\right)\right)}{2\left(\lambda_0^k - \lambda_0^h\right)} - \frac{\sin\left(l_0\left(\lambda_0^k + \lambda_0^h\right)\right)}{2\left(\lambda_0^k + \lambda_0^h\right)}\right]\\
&+ a_0^k b_0^h\left[\frac{\lambda_0^h}{\left(\lambda_0^k\right)^2 - \left(\lambda_0^h\right)^2} + \frac{\cos\left(l_0\left(\lambda_0^k + \lambda_0^h\right)\right)}{2\left(\lambda_0^k + \lambda_0^h\right)} - \frac{\cos\left(l_0\left(\lambda_0^k - \lambda_0^h\right)\right)}{2\left(\lambda_0^k - \lambda_0^h\right)}\right]\\
&+ b_0^k a_0^h\left[\frac{\cos\left(l_0\left(\lambda_0^k + \lambda_0^h\right)\right)}{2\left(\lambda_0^k + \lambda_0^h\right)} + \frac{\cos\left(l_0\left(\lambda_0^k - \lambda_0^h\right)\right)}{2\left(\lambda_0^k - \lambda_0^h\right)} - \frac{\lambda_0^k}{\left(\lambda_0^k\right)^2 - \left(\lambda_0^h\right)^2}\right]\\
&\text{for } k \neq h
\end{aligned}$$

$$\begin{aligned}
\alpha_0^{kk} &= \int_{-l_0}^{0} X_0^k(x) X_0^k(x)\,dx\\
&= \left(a_0^k\right)^2 \int_{-l_0}^{0} \cos^2\left(\lambda_0^k x\right)dx + \left(b_0^k\right)^2 \int_{-l_0}^{0} \sin^2\left(\lambda_0^k x\right)dx\\
&+ 2a_0^k b_0^k \int_{-l_0}^{0} \sin\left(\lambda_0^k x\right)\cos\left(\lambda_0^k x\right)dx\\
&= \left[\left(a_0^k\right)^2 + \left(b_0^k\right)^2\right](l_0/2) + \left[\left(a_0^k\right)^2 - \left(b_0^k\right)^2\right]\\
&\times \frac{\sin\left(2\lambda_0^k l_0\right)}{4\lambda_0^k} - a_0^k b_0^k \frac{\sin^2\left(\lambda_0^k l_0\right)}{\lambda_0^k}
\end{aligned}$$

are computed analytically once. Note that for $t_0 \to 0$ the problem (2.16)–(2.21) is led back to the one presented in [18] and the

solution of (3.8) reduces to $G_k = \exp(-\gamma_0 \lambda_0^2 t)$. Eqs. (3.7)–(3.8) split as a system of linear non-homogeneous ODE's:

$$\begin{aligned}
&\frac{dG_k}{dt} = -\gamma_0\left(\lambda_0^k\right)^2 G_k + \frac{1}{N_k t_0}\left[\beta_0^k \exp(-h_1 t) + \sum_{p=1}^{\infty} \alpha_0^{kp}\left(h_2 H_p(t) - \frac{G_p(t)}{k_0\epsilon_0}\right)\right]\\
&\frac{dH_k}{dt} = -h_1 H_k + G_k\\
&G_k(0) = 0\\
&H_k(0) = 0
\end{aligned} \tag{3.9}$$

3.1. Perturbation solution

A perturbation solution of Eq. (3.9) is developed here as an alternative to the numerical integration.

The coating thickness (l_0) being much smaller (about four orders of magnitude) of the distance d^* where the diffusion takes place ($l_0 \ll d^*$), an asymptotic analysis over l_0 will be carried out, for t_0 large enough. From inspection of their definition

$$N_k = O(1); \qquad \frac{\beta_k}{N_k} = O(l_0); \qquad \frac{\alpha_{kp}}{N_k} = O(l_0)$$

(for simplicity we omit the sub-index 0 from α and β). By setting:

$$\tilde{\beta}_k = \frac{\beta_k}{l_0 N_k} = O(1); \quad \tilde{\alpha}_{kp} = \frac{\alpha_{kp}}{l_0 N_k} = O(1)$$

Eq. (3.9) can be rewritten as

$$\begin{aligned}
&\frac{dG_k}{dt} + \gamma_0\left(\lambda_0^k\right)^2 G_k = \frac{l_0}{t_0}\left[\tilde{\beta}_k \exp(-h_1 t) + \sum_{p=1}^{\infty} \tilde{\alpha}_{kp}\left(h_2 H_p(t) - \frac{G_p(t)}{k_0\epsilon_0}\right)\right]\\
&\frac{dH_k}{dt} + h_1 H_k = G_k
\end{aligned} \tag{3.10}$$

By expanding G_k and H_k as a power series of l_0, i.e.

$$\begin{aligned}
G_k &= G_k^0 + l_0 G_k^1 + l_0^2 G_k^2 + l_0^3 G_k^3 + \cdots\\
H_k &= H_k^0 + l_0 H_k^1 + l_0^2 H_k^2 + l_0^3 H_k^3 + \cdots
\end{aligned} \tag{3.11}$$

substituting in (3.10) and equating terms of the same power, we get, at order 0:

$$\begin{aligned}
&\frac{dG_k^0}{dt} + \gamma_0\left(\lambda_0^k\right)^2 G_k^0 = 0\\
&\frac{dH_k^0}{dt} + h_1 H_k^0 = G_k^0
\end{aligned} \tag{3.12}$$

that, together with the (homogeneous) initial conditions (3.9.3)–(3.9.4), yields

$$G_k^0(t) = 0 \qquad H_k^0(t) = 0 \tag{3.13}$$

Therefore, at order 1, we get

$$\begin{aligned}
&\frac{dG_k^1}{dt} + \gamma_0\left(\lambda_0^k\right)^2 G_k^1 = \frac{\tilde{\beta}_k}{t_0}\exp(-h_1 t)\\
&\frac{dH_k^1}{dt} + h_1 H_k^1 = G_k^1
\end{aligned} \tag{3.14}$$

By enforcing homogeneous initial conditions, we get, if $\gamma_0\left(\lambda_0^k\right)^2 \neq h_1$:

$$G_k^1(t) = \frac{\tilde{\beta}_k}{t_0}\frac{\exp(-h_1 t) - \exp(-\gamma_0\left(\lambda_0^k\right)^2 t)}{\gamma_0\left(\lambda_0^k\right)^2 - h_1}$$

$$H_k^1(t) = \frac{1}{\gamma_0\left(\lambda_0^k\right)^2 - h_1}\left[\frac{\tilde{\beta}_k}{t_0} t\exp(-h_1 t) - G_k^1(t)\right] \tag{3.15}$$

The limiting case $\gamma_0\left(\lambda_0^k\right)^2 \to h_1$ gives the solution

$$G_k^1(t) = \frac{\tilde{\beta}_k}{t_0} t\exp(-h_1 t) \qquad H_k^1(t) = \frac{\tilde{\beta}_k}{t_0}\frac{t^2}{2}\exp(-h_1 t) \tag{3.16}$$

We can now consider the general case for order $n \geqslant 2$. By setting:

$$\mathcal{N}_k^n(t) = \sum_{p=1}^{\infty} \tilde{\alpha}_{kp}\left(h_2 H_p^n(t) - \frac{G_p^n(t)}{k_0\epsilon_0}\right) \tag{3.17}$$

we have:

$$\begin{aligned}
&\frac{dG_k^{n+1}}{dt} + \gamma_0\left(\lambda_0^k\right)^2 G_k^{n+1} = \frac{1}{t_0}\mathcal{N}_k^n\\
&\frac{dH_k^{n+1}}{dt} + h_1 H_k^{n+1} = G_k^{n+1}
\end{aligned}$$

Enforcing initial conditions, we obtain

$$G_k^{n+1}(t) = \frac{1}{t_0}\int_0^t \exp\left[\gamma_0\left(\lambda_0^k\right)^2(\tau - t)\right]\mathcal{N}_k^n(\tau)d\tau$$

$$H_k^{n+1}(t) = \int_0^t \exp[h_1(\tau - t)]G_k^{n+1}(\tau)d\tau \tag{3.18}$$

that give the perturbed solution at the order $n+1$, expressed as a recursive combination of exponential functions of lower order. In the appendix we derive an alternative form for the G_k^2 and H_k^2 in terms of G_k^1 and H_k^1. For their simple analytical form, the first and the second-order expansions (3.15) and (3.18) are likely to be used for t_0 large enough. Results showing the effectiveness of such perturbed solutions will be presented in Section 5.

4. Mass dynamics

The analytical form of the solution given by Eqs. (3.4) and (3.6) allows an easy computation of the dimensionless drug mass (per unit of area) in both coating and wall layers as function of time:

$$M_0^s(t) = (1 - k_0\epsilon_0)\int_{-l_0}^{0} c_0^s(x,t)dx \quad M_i(t) = \int_{x_{i-1}}^{x_i} c_i(x,t)dx$$

$$M_w(t) = \sum_{i=1}^{n} M_i(t)$$

(all masses refer to volume-averaged concentrations, both in fluid- and solid-phases). From Eqs. (3.4)–(3.6) we have:

$$M_0^s(t) = (1 - k_0\epsilon_0)\left(\exp(-h_1 t)l_0 + h_2\sum_k \beta_0^k H_k(t)\right) \tag{4.1}$$

$$\begin{aligned}
M_i(t) &= \sum_k \frac{1}{\left(\lambda_i^k\right)^2}\left[\frac{dX_i^k}{dx}(x_{i-1}) - \frac{dX_i^k}{dx}(x_i)\right]G_k(t)\\
&= \sum_k \frac{a_i^k\left[\sin\left(\lambda_i^k x_i\right) - \sin\left(\lambda_i^k x_{i-1}\right)\right] - b_i^k\left[\cos\left(\lambda_i^k x_i\right) - \cos\left(\lambda_i^k x_{i-1}\right)\right]}{\lambda_i^k}\\
&\quad \times G_k(t) \quad i = 0, 1, \ldots, n
\end{aligned} \tag{4.2}$$

In particular, we have:

$$M_0^s(0) = (1 - k_0\epsilon_0)l_0 \qquad M_i(0) = 0 \qquad i = 0, \ldots, n \tag{4.3}$$

Moreover, from a property of G_k, it follows that $\lim_{t\to\infty} M_i(t) = 0$ for all layers. Nevertheless, for a large enough, yet finite, time, all the mass remains confined in the outermost layer, bounded by the penetration distance (see subsection 2.3). Summing over all the layers 1,2,...,n, the terms that correspond to intermediate layers cancel out and we have:

$$M_w(t) = \sum_k \left[\frac{1}{\left(\lambda_1^k\right)^2} \frac{dX_1^k}{dx}(0) - \frac{1}{\left(\lambda_n^k\right)^2} \frac{dX_n^k}{dx}(1) \right] G_k(t)$$
$$= \sum_k \left[\frac{b_1^k}{\lambda_1^k} - \frac{b_n^k \cos(\lambda_n) - a_n^k \cos(\lambda_n)}{\lambda_n^k} \right] G_k(t) \tag{4.4}$$

We compute the fraction of drug mass retained in each layer (including solid and liquid phase in layer 0), as:

$$\theta_0^s = \frac{M_0^s(t)}{M_0^s(0)} \quad \theta_i(t) = \frac{M_i(t)}{M_0^s(0)} \quad i = 0, 1, \ldots, n \tag{4.5}$$

Having posed the boundary condition (2.14), a negligible mass loss occurs out of the wall bound d^*. In other words, due to the absorbing condition $c_n = 0$, all drug mass is transferred in the outermost layer at a sufficiently large time and the total mass (sum of liquid phase in all layers and of the residual of solid phase in layer 0) is preserved and equals its initial value (say the drug mass in solid phase in coating $M_0^s(0)$) (see section 5):

$$\frac{M_0^s(0) - M_0^s(t) - \sum_{i=0}^n M_i(t)}{M_0^s(0)} = 1 - \theta_0^s(t) - \sum_{i=0}^n \theta_i(t) \simeq 0 \tag{4.6}$$

Thus, any truncation of the domain before d^* is arbitrary and does not ensure a conservative model, because the concentration and the mass flux are not completely damped out (see Eq. (2.14)).

5. Results and discussion

Let us consider the arterial wall subdivided in four layers: endothelium (1), intima (2), IEL (3), and media (4), in contact with the adventitia and external tissues (5). Despite of the low geometrical dimension, a large number of interconnected parameters influence the process and a complete characterization of the physiological data set remains a difficult task. In this paper, we focus on the dependence of the concentration and mass profiles on the phase transfer characteristic time t_0. To set up a realistic simulation, the parameters given in Table 1 and the values

$$P = 10^{-6}\text{cm/s} \qquad d^* = 1 \text{ cm} \tag{5.1}$$

have been chosen in agreement with the typical scales in DES and data in literature for the arterial wall and heparin drug in the coating layers [13]. Here, these values are left unchanged as reference

Table 1
The parameters used in the simulations for the coating and the wall layers. The penetration distance d^* estimates the wall bound, provides the thickness l_5 of the external layer and depends on the maximum simulated time.

	Coating (0)	Endothelium (1)	Intima (2)	IEL (3)	Media (4)	Adventitia (5)
$l_i = x_i - x_{i-1}(cm)$	$5 \cdot 10^{-4}$	$2 \cdot 10^{-4}$	10^{-3}	$2 \cdot 10^{-4}$	$2 \cdot 10^{-2}$	$d^* - x_4$
$D_i(cm^2/s)$	10^{-10}	$8 \cdot 10^{-9}$	$7.7 \cdot 10^{-8}$	$4.2 \cdot 10^{-8}$	$7.7 \cdot 10^{-8}$	$12 \cdot 10^{-8}$
ϵ_i	0.1	$5 \cdot 10^{-4}$	0.61	$4 \cdot 10^{-3}$	0.61	0.85
k_i	1	1	1	1	1	1

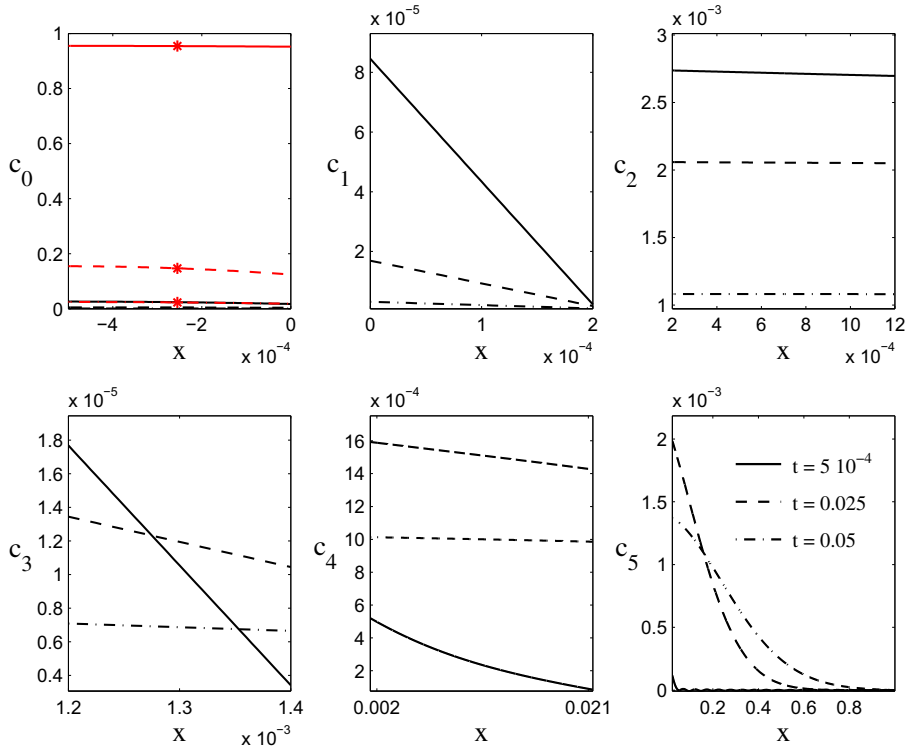

Fig. 3. Concentration profiles in the six layers at three instants, for $t_0 = 10^{-3}$ (note the different scale for coordinates and concentrations). In the coating (top left), both solid (red starred) and liquid (black) phase concentration are depicted. (For interpretation of the references to colour in this figure caption, the reader is referred to the web version of this article.)

Table 2
Relative L^2 norm error (as in Eq. (5.2)) between the numerical and the first- and second-order perturbed solutions.

t_0	Err (G_1)	Err (G_2)	Err (H_1)	Err (H_2)
10^{-3}	0.26	0.089	0.191	0.054
10^{-1}	0.004	$3.35 \cdot 10^{-4}$	0.009	0.005
1	0.0015	0.0015	0.001	0.0006

Table 3
Percentage of the drug mass retained in each layer at different times for $t_0 = 10^{-4}$.

t (adim.)	t (dim.) d:h:m	θ_0^s	θ_0	θ_1	θ_2	θ_3	θ_4	θ_5
10^{-4}	13 m	92	5.9	< 0.01	0.7	< 0.01	0.2	< 0.01
$5 \cdot 10^{-4}$	1 h:9 m	83	7.5	< 0.01	2.1	< 0.01	4.9	1.5
$5 \cdot 10^{-3}$	11 h:34 m	34	3.1	< 0.01	1.4	< 0.01	12.9	48
$5 \cdot 10^{-2}$	4*d*:17 h	0.1	0.01	< 0.01	0.1	< 0.01	3.8	95

parameters. We are interested to investigate the effect of t_0 only, in order to understand the relative importance of solid–liquid mass transfer on the release process. All the series appearing in the solution (see Eq. (3.4) and following) have been truncated at a number of terms $m = 50$. The outermost layer results much thicker than the others and needs a higher number of base points to be conveniently resolved.

We compute the functions $G_k(t)$ and $H_k(t)$ by solving the system of ODE's (3.9) with a numerical method based on a 4-th order Runge–Kutta scheme. Because of a possible stiffness, an adaptive time step over a sequence of times t_j, $j = 1, 2, \ldots, v$ is used. For t_0 large enough, the perturbed solutions ψ_1^P and ψ_2^P are shown to have a sufficient accuracy. The numerical solution ψ^N will be used for comparative purposes and the relative error measured as:

$$\mathrm{Err}(\phi) = \frac{\|\psi^P - \psi^N\|}{\|\psi^N\|} = \frac{\left[\sum_{k=1}^{M}\sum_{j=1}^{v}\left(\psi_k^P(t_j) - \psi_k^N(t_j)\right)^2\right]^{1/2}}{\left[\sum_{k=1}^{M}\sum_{j=1}^{v}\psi_k^N(t_j)^2\right]^{1/2}} \qquad (5.2)$$

where the first and second-order perturbed solutions are respectively (cfr Eq. (3.11)):

$$\psi_1^P = \psi^0 + l_0\psi^1 \qquad \psi_2^P = \psi^0 + l_0\psi^1 + l_0^2\psi^2$$

Table 2 shows the discrepancy between the numerical and the perturbation solution for three values of t_0 with the same M and v. The perturbed solution deteriorates for $t_0 \lesssim 10^{-3}$ and more terms of the expansion are necessary. On the other hand, the perturbed solution converges for $t_0 \gtrsim 1$ proving that the first- and second-order approximation are sufficient to catch up the whole solution.

Results from the LMNE model show that the concentration is decreasing inside each layer, being possibly discontinuous at the interfaces, with the mass flux continuity preserved. Interestingly enough, the levels of volume-averaged drug concentration in layer 2 (intima) are nearly constant and can be higher than in the others, at intermediate times. This is in agreement with the higher diffusivity D_2 and relatively small layer thickness l_2. The drug distribution shows a strong dependence on the transfer time t_0 (Fig. 3).

It can be seen that drug is differently retained in each layer, which receives mass from the inner and transmits to the outer, in a cascade sequence, up to be completely damped out at distance d^* that constitutes the wall bound. From Fig. 4 it turns out that the solid-phase mass is exponentially decreasing in the coating, while the liquid- phase is first increasing up to some

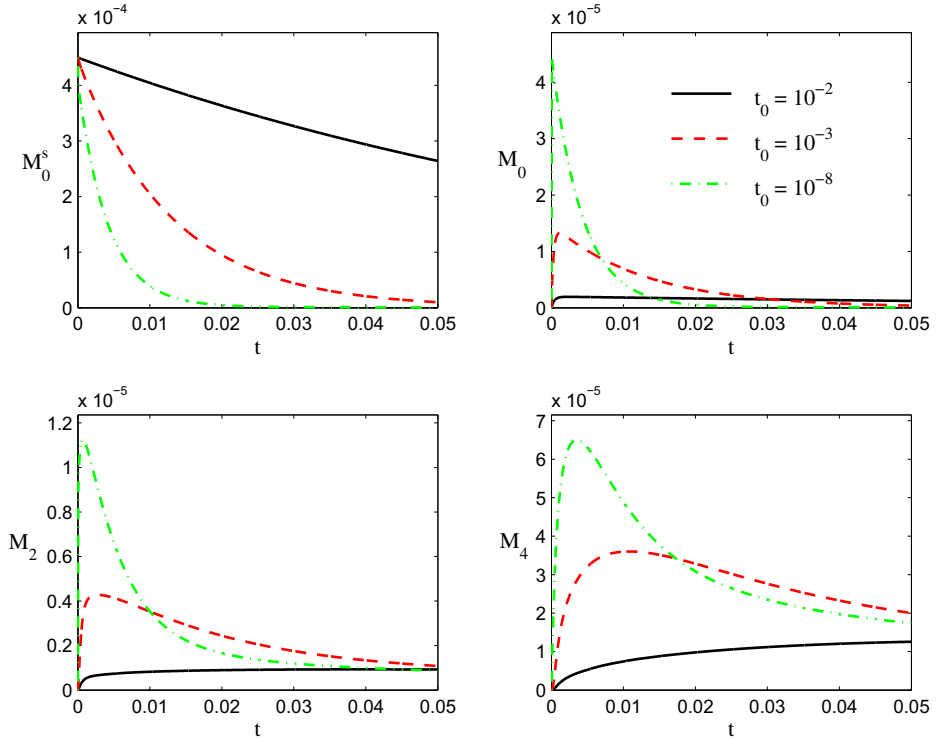

Fig. 4. Drug mass in the coating (layer 0, solid and liquid phase), intima (layer 2) and media (layer 4) as a function of time, for three values of t_0. Only the solid-phase mass is monotonically decreasing in the coating, while the liquid-phase mass has a characteristic time at which the drug reaches a peak in each layer. The velocity of the coating depletion, the location and the magnitude of the peak critically depend on the transfer time t_0.

Table 4
Percentage of the drug mass retained in each layer at different times for $t_0 = 10^{-2}$. Note the slower release and the moderate absorption with respect to the previous case. The coating emptying rate is greatly reduced.

t (adim.)	t (dim.) d:h:m	θ_0^s	θ_0	θ_1	θ_2	θ_3	θ_4	θ_5
10^{-4}	13 m	99	0.09	< 0.01	0.01	< 0.01	< 0.01	< 0.01
$5 \cdot 10^{-4}$	1 h:9 m	99	0.3	< 0.01	0.07	< 0.01	0.12	0.03
$5 \cdot 10^{-3}$	11 h:34 m	94	0.4	< 0.01	0.1	< 0.01	1.1	3.4
$5 \cdot 10^{-2}$	4*d*:17 h	58	0.2	< 0.01	0.2	< 0.01	2.7	38

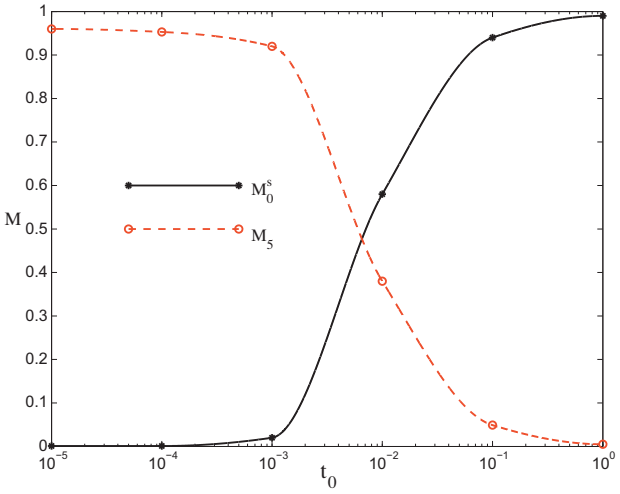

Fig. 5. Drug mass at time $t = 0.05$ in the coating at solid phase (continuous line) and the adventitial layer (dashed line) as a function of t_0. It is seen that at very low t_0 drug is quicky released through the DES to the tissue, while the release is much slower at $t_0 \geqslant 0.1$.

upper bound and then decaying asymptotically in all layers. At the first instants, the process is dominated by solid–liquid transfer process and mass raises up to a peak value, while, at later times, diffusion dominates. The location and the magnitude of the peak influence the characteristics of the drug dynamics and is critically dependent on the transfer time t_0 (Fig. 4). As expected, the differences increase with t_0 and are more marked at early times and in the first layers, while the mass profiles tend to coincide at later times and in the outermost layers. It is also evident that for $t_0 \to 0$ the behaviour of the solution (inasmuch as $t \gg t_0$) tends to that of model [18], where an instantaneous mass transfer and a correspondent initial condition are imposed (Fig. 4).

To measure the release rate and the different absorption rate with the wall depth, we compute the fraction of drug retained in each layer as in Eq. (4.5): the layers 1 and 3 retain a negligible mass due to their thickness, whereas the drug accumulates in the outermost layer (5) as the time proceeds. At a time large enough, all the mass is transferred to the external wall layer, with a negligible loss. However, the therapeutic effects of DES is limited in the endothelium – media, while the residual drug in the outmost layer is considered lost. Tables 3 and 4 show the different distribution in the coating and in the wall layers for two values of t_0. Looking at the more favorable case ($t_0 = 10^{-2}$, Table 4), it is shown a delayed emptying of the coating and a slower release in all layers.

A smaller t_0 is responsible for a faster solid–liquid transfer in the polymer and a quicker diffusion in the other layers, while a larger t_0 ensures a prolonged release and a more uniform distribution. Fig. 5 shows how rapid is the response of the DES (measured through the level of mass present at coating and adventitial layer at a given time) to the solid–liquid transfer time. It is shown that for $t_0 < 10^{-3}$ the transfer is extremely fast and occurs almost instantaneously. On the other way around, for $t_0 > 1$ the transfer results quite slow and the whole mass remains in the coating at solid phase, all the dynamics being hampered (cfr. Fig. 4). A technologically advanced DES should guarantee an optimal release, and this is controlled by a suitable drug solid–liquid transfer time. Therefore, for the set of parameters chosen here, t_0 remains in the range $[0.01, 0.1]$ (that corresponds to a characteristic solid–fluid transfer time of 1–10 days): picking a value in such an interval, a controlled and effective drug release takes place.

6. Concluding remarks

Manufacturing of drug delivery system with consistent and reproducible elution is a great challenge in today's biomechanical engineering. A deeper understanding of drug release kinetics is necessary for rational design of stent-based drug delivery system to optimize therapeutic efficacy and minimize local vascular toxicity. One of the methods to evaluate the characteristics of drug elution from the coating into the vascular wall and to optimize the physico-chemical parameters is the mathematical modelling and the numerical simulation. It is important to design drug release kinetics such that the therapeutic effects cover the timeline of the vessel wall remodelling. As a matter of fact, a correct evaluation of the drug dynamics inside the polymeric matrix is a starting point for the efficacy of the whole delivery process.

In this paper a LMNE model for mass dynamics from a DES has been developed to study the relative influence of the various factors affecting the drug release: the significant parameter we focused here is the mass transfer time which captures the solid–liquid phase dynamics and depends on the microstructure of the porous polymeric coating, combined with the chemo–physical properties of the drug. It has been shown to which extent this characteristic time influences the release process. Thus, the presented model offers a useful tool for predicting concentration profiles from different porous coating platforms and for devising novel kinetics for other drug delivery systems. Results of LME models generally underestimate the release time and models that include non- equilibrium mass transfer processes can lead to more accurate results that can have a significant impact in stent design.

The model contains several parameters that need to be identified before it can be used in a predictive way and provide the significant kinetics. Having done that, the proposed methodology can be used to quantitatively characterize the drug elution, to improve the technological performance and shows how the release rate can be optimized for therapeutic purposes.

Acknowledgments

This study was partially supported by the MIUR-CNR project "Interomics", 2012–2013.

Appendix

We develop here the analytical (recursive) form for the first- and second-order perturbation solution given in Subs 3.1. Let us first define the three argument function:

$$\mathcal{G}(\xi,\eta,t)\equiv\frac{\exp(-\xi t)-\exp(-\eta t)}{\xi-\eta} \tag{A.1}$$

having the following properties:

$$\mathcal{G}(\xi,\eta,t)=\mathcal{G}(\eta,\xi,t)\qquad \lim_{\xi\to\eta}\mathcal{G}(\xi,\eta,t)=-t\exp(-\eta t)\equiv\mathcal{G}(\eta,\eta,t)$$
$$\frac{\partial\mathcal{G}(\xi,\eta,t)}{\partial\xi}=\frac{\mathcal{G}(\xi,\xi,t)-\mathcal{G}(\xi,\eta,t)}{\xi-\eta}\qquad \frac{\partial\mathcal{G}(\xi,\eta,t)}{\partial\eta}=\frac{\mathcal{G}(\eta,\eta,t)-\mathcal{G}(\xi,\eta,t)}{\xi-\eta}$$
$$\frac{\partial\mathcal{G}(\xi,\eta,t)}{\partial\eta}=\frac{\partial\mathcal{G}(\eta,\xi,t)}{\partial\xi}$$

It can also be seen that:

$$\lim_{\eta\to\xi}\frac{\partial\mathcal{G}(\xi,\eta,t)}{\partial\xi}=\lim_{\eta\to\xi}\frac{\partial\mathcal{G}(\xi,\eta,t)}{\partial\eta}=\frac{t^2}{2}\exp(-\xi t)=\frac{t}{2}\mathcal{G}(\xi,\xi,t) \tag{A.2}$$

By this function $\mathcal{G}$, we can rewrite G_k^1 and H_k^1 in Eq. (3.15) in a compact form as:

$$G_k^1(t)=-\frac{\tilde\beta_k}{t_0}\mathcal{G}(h_1,\gamma_0\left(\lambda_0^k\right)^2,t)$$

$$H_k^1(t)=\frac{\tilde\beta_k}{t_0}\frac{\partial\mathcal{G}\left(h_1,\gamma_0\left(\lambda_0^k\right)^2,t\right)}{\partial\left(\gamma_0\left(\lambda_0^k\right)^2\right)} \tag{A.3}$$

with the limiting case $h_1\to\gamma_0\left(\lambda_0^k\right)^2$ included.

Similarly, the computation of second-order term developed in Subs 3.1 can be given in an explicit form. It is easy to verify that:

$$I(\xi,\eta,\zeta,t)\equiv\int_0^t\exp(\zeta(\tau-t))\mathcal{G}(\xi,\eta,\tau)d\tau=\frac{\mathcal{G}(\xi,\zeta,t)-\mathcal{G}(\eta,\zeta,t)}{\xi-\eta} \tag{A.4}$$

with

$$\lim_{\xi\to\eta}I(\xi,\eta,\zeta,t)=\frac{\partial\mathcal{G}(\eta,\zeta,t)}{\partial\xi}$$

and

$$J(\xi,\eta,\zeta,t)=\int_0^t\exp(\zeta(\tau-t))\frac{\partial\mathcal{G}(\xi,\eta,\tau)}{\partial\eta}d\tau=\frac{I(\eta,\eta,\zeta,t)-I(\xi,\eta,\zeta,t)}{\xi-\eta} \tag{A.5}$$

We also estimate convolution integrals:

$$I_H(\xi,\eta,\zeta,t)=\int_0^t\exp(\xi(\tau-t))I(\xi,\eta,\zeta,t)d\tau=\frac{I(\xi,\xi,\zeta,t)-I(\xi,\eta,\zeta,t)}{\xi-\eta} \tag{A.6}$$

and

$$J_H(\xi,\eta,\zeta,t)=\int_0^t\exp(\xi(\tau-t))J(\xi,\eta,\zeta,t)=\frac{-J(\eta,\xi,\zeta,t)-I_H(\xi,\eta,\zeta,t)}{\xi-\eta} \tag{A.7}$$

Note that $\mathcal{G}$ (resp. I,J) can be viewed as divided differences of first- (resp. second-) order over exponential functions, having t as a parameter. From Eq. (3.17) we have:

$$\mathcal{N}_k^1(\tau)=\sum_{p=1}^{\infty}\tilde\alpha_{kp}\left(h_2H_p^1(\tau)-\frac{G_p^1(\tau)}{k_0\epsilon_0}\right)=\frac{1}{t_0}\sum_{p=1}^{\infty}\tilde\alpha_{kp}\tilde\beta_p\left(h_2\frac{\partial\mathcal{G}\left(h_1,\gamma_0\left(\lambda_0^p\right)^2,t\right)}{\partial\left(\gamma_0\left(\lambda_0^p\right)^2\right)}+\frac{1}{k_0\epsilon_0}\mathcal{G}\left(h_1,\gamma_0\left(\lambda_0^p\right)^2,t\right)\right) \tag{A.8}$$

Finally, by evaluating Eq. (3.18) for $n=1$, we get:

$$G_k^2(t)=\frac{1}{t_0}\sum_{p=1}^{\infty}\tilde\alpha_{kp}\tilde\beta_p\left(h_2J\left(h_1,\gamma_0\left(\lambda_0^p\right)^2,\gamma_0\left(\lambda_0^k\right)^2,t\right)+\frac{1}{k_0\epsilon_0}I(h_1,\gamma_0\left(\lambda_0^p\right)^2,\gamma_0\left(\lambda_0^k\right)^2,t)\right)$$

$$H_k^2(t)=\frac{1}{t_0}\sum_{p=1}^{\infty}\tilde\alpha_{kp}\tilde\beta_p\left(h_2J_H\left(h_1,\gamma_0\left(\lambda_0^p\right)^2,\gamma_0\left(\lambda_0^k\right)^2,t\right)+\frac{1}{k_0\epsilon_0}I_H\left(h_1,\gamma_0\left(\lambda_0^p\right)^2,\gamma_0\left(\lambda_0^k\right)^2,t\right)\right) \tag{A.9}$$

References

[1] A.R. Tzafriri, A. Groothuis, G.S. Price, E.R. Edelman, Stent eluting rate determines drug deposition and receptor-mediated effects, J. Controll. Release 161 (2012) 918–926.
[2] W.H. Maisel, Unanswered questions: Drug-eluting stents and the risk of late thrombosis, New Engl. J. Med. 356 (2007) 981–984.
[3] C. Hwang, D. Wu, E.R. Edelman, Physiological transport forces govern drug distribution for stent- based delivery, Circulation 104 (5) (2001) 600–605.
[4] R. Mongrain, L. Faik, et al., Effects of diffusion coefficients and struts apposition using numerical simulations for drug eluting coronary stents, J. Biomech. Eng. 129 (2007) 733–742.
[5] P. Zunino, C. D'Angelo, L. Petrini, C. Vergara, C. Capelli, F. Migliavacca, Numerical simulation of drug eluting coronary stents: mechanics, fluid dynamics and drug release, Comput. Methods Appl. Mech. Eng. 198 (2009) 3633–3644.
[6] J.M. Weiler, E.M. Sparrow, R. Ramazani, Mass transfer by advection and diffusion from a drug-eluting stent, Int. J. Heat Mass Transfer 55 (2012) 1–7.
[7] G.A. Truskey, F. Yuan, D.F. Katz, Transport phenomena in biological system, Pearson Prent. Hall, 2010.
[8] G. Vairo, M. Cioffi, R. Cottone, G. Dubini, F. Migliavacca, Drug release from coronary eluting stents: a multidomain approach, J. Biomech. 43 (8) (2010) 1580–1589.
[9] S. McGinty, S. McKee, R.M. Wadsworth, C. McCormick, Modelling drug-eluting stents, Math. Med. Biol. 28 (2011) 1–29.
[10] S. Hossainy, S. Prabhu, A mathematical model for predicting drug release from a biodurable drug-eluting stent coating, J. Biomed. Mater. Res. A 87 (2) (2008) 487–493.
[11] H.Q. Zhao, D. Jayasinghe, S. Hossainy, L.B. Schwartz, A theoretical model to characterize the drug release behaviour of drug-eluting stents with durable polymer matrix coating, J. Biomed. Mater. Res. A 100 (2012) 120–124.
[12] S. Prabhu, Computational modeling in stent-based drug delivery, Briefing: Med. Device Manuf. Technol. (2004) 1–4.
[13] C.J. Creel, M.A. Lovich, E.R. Edelman, Arterial paclitaxel distribution and deposition, Circ. Res. 86 (8) (2000) 879–884.
[14] M. Khakpour, K. Vafai, A critical assessment of arterial transport models, Int. J. Heat Mass Transfer 51 (2008) 807–822.
[15] Y. Davit, G. Debenest, B.D. Wood, M. Quintard, Modeling non-equilibrium mass transport in biologically reactive porous media, Adv. Water Res. 33 (2010) 1075–1093.
[16] G. Pontrelli, F. de Monte, Mass diffusion through two-layer porous media: an application to the drug-eluting stent, Int. J. Heat Mass Transfer 50 (2007) 3658–3669.
[17] G. Pontrelli, F. de Monte, Modeling of mass dynamics in arterial drug-eluting stents, J. Porous Media 12 (1) (2009) 19–28.
[18] G. Pontrelli, F. de Monte, A multi-layered porous wall model for coronary drug-eluting stents, Int. J. Heat Mass Transfer 53 (2010) 3629–3637.
[19] A.C. Guyton, J.E. Hall, Textbook of Medical Physiology, 11th ed., Elsevier, 2007.

[20] S. Wang, K. Vafai, Analysis of the effect of stent emplacement on LDL transport within an artery, Int J. Heat Mass Transfer (2013) 1031–1040.
[21] K. Vafai (Ed.), Porous Media: Applications in Biological Systems and Biotechnology, Taylor & Francis, 2010.
[22] F. de Monte, G. Pontrelli, S.M. Becker, Drug release in biological tissues, Chapt. 3, in: S.M. Becker, A.V. Kuznetsov (Eds.), Transport in Biological Media, Elsevier, New York, 2013, pp. 59–118.
[23] B.B. Dykaar, P.K. Kitanidis, Macrotransport of a biologically reacting solute through porous media, Water Resource Res. 32 (2) (1996) 307–320.
[24] H.D. Baehr, K. Stephan, Heat and Mass Transfer, Springer, Berlin, 1998.
[25] A. Kargol, M. Kargol, S. Przestalski, The Kedem-Katchalsky equations as applied for describing substance transport across biological membranes, Cell. Mol. Biol. Lett. 2 (1996) 117–124.